Application of Timoshenko Beam-Column Theory in Data Correction for Steel Beam-Column Testing

Piyachai Chansuk[1]; Gulen Ozkula, Ph.D.[2]; and Chia-Ming Uang, Ph.D., M.ASCE[3]

Abstract: A recent cyclic test program evaluated the performance of steel wide-flange columns under axial loads and lateral drifts; the specimens had either fixed-fixed or fixed-rotating boundary conditions. For both cases, the flexibility of fully restrained moment connections at specimen ends, which varied in degrees based on several factors such as configurations of the bolted connection, end-plate thickness, and magnitude of the applied axial load, was observed to have significant impacts on elastic flexural stiffnesses of the measured responses. Therefore, the measured responses needed to be corrected, accounting for the effects of connection flexibility, before test parameters of interest can be investigated. A data-correction procedure that eliminates the effect of connection flexibility from the measured beam-column responses is developed. The procedure is built upon theoretical knowledge of elastic Timoshenko beam-column behavior. Once the effect of connection flexibility is removed, the corrected test responses become equivalent to the responses of beam-columns with ideal rigid end connections. **DOI: 10.1061/(ASCE)ST.1943-541X.0002533.**

Author keywords: Beam-column cyclic tests; Connection flexibility; Data correction; Timoshenko beam-column; Elastic flexural stiffnesses.

Introduction

Steel special moment frames (SMFs) are one of the most commonly used lateral force–resisting systems in high seismic regions due to their high energy-dissipation capacity and architectural versatility. To achieve ductility in the seismic response of a multistory SMF, design requirements in AISC 341 (AISC 2016b) and AISC 358 (AISC 2016a) intend to provide significant inelastic deformation capacity through flexural yielding in the beams and limited shear yielding of column panel zones. Although strong column-weak beam design requirements are also provided, flexural yielding or plastic hinging at the base of the first-story columns is unavoidable and permitted by AISC 341.

Design engineers sometimes refer to wide-flange columns with nominal depths greater than 356 mm (14 in.) as deep columns and those with lower nominal depths as shallow columns. Deep wide-flange columns (e.g., W24–W36) are preferred in the designs of SMF, especially after the 1994 Northridge Earthquake, to achieve economy while attaining a high lateral stiffness required to satisfy story drift limits of the building codes (ASCE 2016). Despite this popularity in the designs, limited research has been conducted to study cyclic inelastic behavior of deep columns under both the axial and flexural demands for seismic applications. To fill this knowledge gap, NIST (2011) initiated a comprehensive research program to evaluate the usage of deep columns in SMFs and its effects on the seismic response at the member, beam-column subassembly, and system levels.

In the designs of braced frames, shallow wide-flange columns are commonly used. Newell and Uang (2008) tested shallow (W14) columns under varying axial load and cyclic story drifts and reported excellent member ductility capacity even when the axial load was high (up to 70% of the member yield strength). Because deep columns usually have much larger section slenderness parameters (i.e., width-to-thickness ratios h/t_w and $b_f/2t_f$, where h is web depth, t_w is web thickness, b_f is flange width, and t_f is flange thickness) for web local buckling (WLB) and flange local buckling (FLB) limit states as well as a larger member slenderness parameter (i.e., L/r_y, where L is member length, and r_y is radius of gyration about the weak axis) for lateral-torsional buckling and flexural buckling limit states, it is not clear if the same conclusion on shallow column behavior can be generalized to deep columns. As part of the NIST research program, full-scale steel wide-flange (W18 to W30 shapes) columns were tested with axial forces and cyclic lateral drifts to evaluate their hysteretic responses and buckling behaviors for seismic applications (Ozkula and Uang 2017; Chansuk et al. 2018).

In this test program, the specimens had either fixed-fixed or fixed-rotating boundary conditions. For both cases, it was observed that the measured beam-column responses, especially in the elastic range, were sensitive to flexibility of the fully restrained moment connections that fixed the specimen ends. Correspondingly, this connection flexibility became another unintended variable that influenced the test responses, hindering investigation of parameters of interest in this research. Thus, a data-correction procedure is needed to eliminate the effect of connection flexibility from the measured beam-column responses and enable meaningful response investigations.

The first part of this paper briefly discusses the test program, sample test results, and the challenges in analyzing test data that arise from the effects of connection flexibility. Subsequently, a data-correction procedure is proposed to overcome the challenges. A literature review of classical beam-column theories then follows to present available closed-form formulas for determining

[1]Structural Designer, John A. Martin and Associates, Los Angeles, CA 90015. ORCID: https://orcid.org/0000-0002-3577-6015. Email: pchansuk@johnmartin.com

[2]Assistant Professor, Dept. of Civil Engineering, Namik Kemal Univ., Tekirdağ 59860, Turkey. Email: gozkula@nku.edu.tr

[3]Professor, Dept. of Structural Engineering, Univ. of California, San Diego, La Jolla, CA 92093 (corresponding author). ORCID: https://orcid.org/0000-0002-8467-9748. Email: cmu@ucsd.edu

Note. This manuscript was submitted on November 16, 2018; approved on July 18, 2019; published online on December 31, 2019. Discussion period open until May 31, 2020; separate discussions must be submitted for individual papers. This paper is part of the ***Journal of Structural Engineering***, © ASCE, ISSN 0733-9445.

Table 1. Test specimens with fixed-fixed boundary conditions

Specimen No.	Shape	L (m)	P (kN)	μ ($\times 10^{-3}$)	K_e (kN/mm)	K_{me} (kN/mm)	β	K_θ (GN · m/rad)	Stiffness reduction[a] (%)
1L	W24 × 176	5.49	2,064	2.46	27.62	19.97	13.00	1.21	27.7
1M	W24 × 176	5.49	4,132	4.93	27.19	21.65	19.75	1.70	20.4
1H	W24 × 176	5.49	6,205	7.40	26.76	21.90	22.84	1.97	18.2
2L	W24 × 131	5.49	1,544	2.28	19.99	14.27	12.72	0.78	28.6
2M	W24 × 131	5.49	3,100	4.57	19.67	16.17	23.94	1.46	17.8
2H	W24 × 131	5.49	4,617	6.81	19.35	15.35	19.92	1.21	20.7
3L	W24 × 104	5.49	1,214	2.17	15.59	12.60	21.78	1.02	19.2
3M	W24 × 104	5.49	2,438	4.35	15.33	13.01	29.32	1.38	15.2
3H	W24 × 104	5.49	3,661	6.53	15.08	12.78	29.31	1.38	15.3
4L	W24 × 84	5.49	974	1.85	12.26	10.59	33.44	1.20	13.7
4M	W24 × 84	5.49	1,971	3.75	12.05	10.76	44.59	1.60	10.8
5L	W24 × 55	5.49	636	1.44	7.28	6.63	56.36	1.15	8.9
5LM	W24 × 55	5.49	979	2.21	7.21	6.75	85.17	1.74	6.4
5M	W24 × 55	5.49	1,130	2.55	7.17	6.83	82.88	1.70	4.7
11M	W24 × 176	5.33	4,097	4.89	29.33	23.11	18.43	1.63	21.2
12LM	W30 × 261	5.33	4,613	3.53	62.80	42.69	9.61	1.96	32.0
13M	W30 × 173	5.33	4,066	4.43	40.35	31.03	15.71	2.02	23.1
14L	W30 × 90	5.38	1,054	1.60	19.20	16.93	37.71	2.10	11.9
15L	W18 × 192	5.38	2,246	2.79	20.76	17.00	23.75	1.42	18.1
16M	W18 × 130	5.38	3,043	5.42	13.02	11.19	33.20	1.26	14.0
17L	W18 × 76	5.38	876	2.47	7.35	6.87	78.66	1.62	6.5
22L	W30 × 148	5.49	1,730	1.89	32.16	25.16	17.63	1.79	21.8
23L	W18 × 60	4.27	689	1.99	10.76	9.78	52.34	1.00	9.1
24L	W14 × 82	4.27	947	2.97	9.58	8.21	32.14	0.55	14.2
25L	W14 × 53	4.27	609	2.64	6.00	5.61	79.69	0.84	6.4
26LM	W14 × 132	4.27	2,313	5.72	15.67	13.43	30.81	0.92	14.3
27L	W24 × 84	5.49	974	1.85	12.26	10.69	35.90	1.29	12.9

[a]Stiffness reduction = $(K_e - K_{me})/K_e$.

theoretical elastic flexural stiffnesses of beam-columns with rigid end connections. Application of the theoretical formulas to correct test responses of beam-column specimens with fixed-fixed boundary conditions is presented next. For specimens tested with fixed-rotating boundary conditions, flexibility of end moment connections does not only affect the member stiffnesses but also change their internal force distribution. Due to this complexity, close-formed formulas that express the behavior of Timoshenko beam-columns with flexible end connections are required to examine the specimen responses. These expressions, which are not available in literatures, are derived in this paper in a classical manner and applied to the data-correction procedure for fixed-rotating tests.

NIST Test Program

Parameters Investigated

Columns tested in this research were intended to represent the first-story columns in a multistory SMF. Table 1 presents the test matrix; the numbers preceding the specimen labels indicate specimen groups. In the first phase of this test program, Ozkula and Uang (2015, 2017) tested five W24 shapes (Groups 1–5) of ASTM A992 steel for a total of 14 specimens to investigate the effects of section and member slenderness parameters on the strong-axis flexural responses and buckling behaviors. The applied axial force was kept constant in each test to simulate the response of an interior column. To study the effects of axial load levels on the failure mode, column ductility capacity, and axial shortening, each specimen group, with a few exceptions, consisted of three specimens of the same shape undergoing low ($0.18P_y$), medium ($0.36P_y$), and high ($0.54P_y$) levels of axial compression, where P_y = nominal yield strength of column; letters L, M, and H indicate these axial load levels, respectively, in the specimen labels. Fully restrained moment connections were used at both ends of the specimens; the intent was to simulate fixed-fixed boundary conditions. Although most specimens underwent strong-axis cyclic bending, some specimens such as Specimen 6L were subjected to weak-axis cyclic bending to investigate the effects of bending direction.

Chansuk et al. (2018) tested 11 additional wide-flange shapes (Groups 11–27) ranging from W14–W30 for a total of 13 specimens with strong-axis bending in the second phase of the test program. The objectives were to (1) further examine the parameters investigated in the first phase of testing, (2) determine whether findings from testing of W24 specimens in the first phase could be extrapolated to deeper (e.g., W30) and shallower (e.g., W14 and W18) shapes with similar section slenderness parameters, and (3) expand the experimental database. In addition, the effects of boundary conditions were investigated; a fixed-rotating loading protocol (discussed in a subsequent section) was imposed to some specimens (Table 2). Other parameters such as biaxial bending, lateral drift loading sequences, and varying axial loads were also studied in this test program but are outside the scope of this paper.

Test Setup

Testing was conducted in the Seismic Response Modification Device (SRMD) Test Facility at the University of California, San Diego, with the test setup as shown in Fig. 1. Specimens were tested in a horizontal position; L indicates their clear lengths (Tables 1 and 2). The west end of the specimens was connected to a reaction fixture that was fixed to a strong wall. The east or moving end was connected to a reaction fixture that was tied down to the SRMD moving platen, simulating a column top end that

Table 2. Test specimens with fixed-rotating boundary conditions

Specimen No.	Shape	L (m)	ξ_m	P (kN)	μ ($\times 10^{-3}$)	β	K_θ (GN · m/rad)	x_{IP} (mm)	ξ	K_e (kN/mm)	K_{me} (kN/mm)	Stiffness reduction[a] (%)
11H-BC	W24 × 176	5.33	1.12	6,196	7.40	23.49	2.08	1,104	1.17	11.27	9.75	13.4
13M-BC	W30 × 173	5.33	1.00	4,066	4.43	17.20	2.21	1,343	1.06	18.54	15.49	16.4
16M-BC	W18 × 130	5.38	1.00	3,060	5.45	33.56	1.28	1,565	1.04	5.94	5.32	10.5

[a]Stiffness reduction $= (K_e - K_{me})/K_e$.

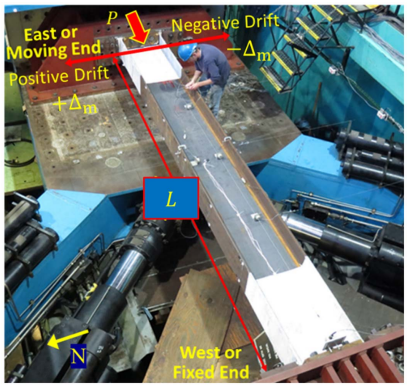

Fig. 1. Test setup.

swayed (and rotated for the fixed-rotating loading case) during a seismic event.

To achieve fully restrained moment connections at both ends, bolted end-plate connections [ASTM A572 Grade 50 (ASTM 2018)] were used in this test program (Fig. 2). They were fastened to the reaction fixtures with 38-mm diameter high-strength pretensioned threaded rods [ASTM A354 Grade BD (ASTM 2017)]. Table 3 summarizes the connection details for each specimen group, including the dimensions of the end plate and the number of bolts at each end.

With this test setup, longitudinal movements of the platen, which were force-controlled, imposed a targeted axial force, P, to the specimen. Applied (i.e., measured) cyclic lateral displacement, Δ_m, of the platen in the horizontal plane imposed double-curvature strong-axis bending to the specimens. Cyclic rotations, θ_m, of the platen about the member strong axis simulated top end rotation of the first-story columns in a SMF. The platen was in a displacement-control mode for the lateral and strong-axis rotational movements.

Testing Procedure and Loading Protocols

Figs. 3(a) and 4(a) show the ideal fixed-fixed and fixed-rotating boundary conditions intended in testing of the specimens listed in Tables 1 and 2, respectively. An axial force was applied first in these tests and maintained at a targeted magnitude throughout the cyclic loading. For fixed-fixed tests, only cyclic lateral drifts were imposed at the moving end of the specimen, i.e., the top end of the first-story column in a moment frame in perspective. Typical in this test program, the symmetrical cyclic lateral drift loading protocol for qualifying cyclic tests of beam-to-column moment connections in special and intermediate moment frames specified in Section K2.4b of AISC 341 (AISC 2016b) was used. Fig. 5(a) shows the sequence of this AISC loading protocol in term of story drift angle, Δ_m/L.

For specimens tested with the fixed-rotating boundary conditions, cyclic end rotations [Fig. 5(b)] in-phase with and proportional to the AISC lateral drift sequence [Fig. 5(a)] were also applied to the moving end of the column specimens. For this test program, the applied end rotations were expressed as follows:

$$\theta_m = \xi_m \left(\frac{\Delta_m}{L}\right) \tag{1}$$

A three-bay, 4-story SMF designed by Harris and Speicher (2015) was analyzed to determine an appropriate ξ_m value for this test program. Based on nonlinear time-history analyses of this structure with 14 ground motions, scaled to match the Design Earthquake per ASCE 7 (ASCE 2016), the top end rotations and the first-story drift angles were similar in magnitude. Values of ξ_m used in this test program are summarized in Table 2; ξ_m was initially set to 1 for all fixed-rotating specimens but due to human error, Specimen 11H-BC with W24 × 176 shape was tested with a slightly larger ξ_m value of 1.12.

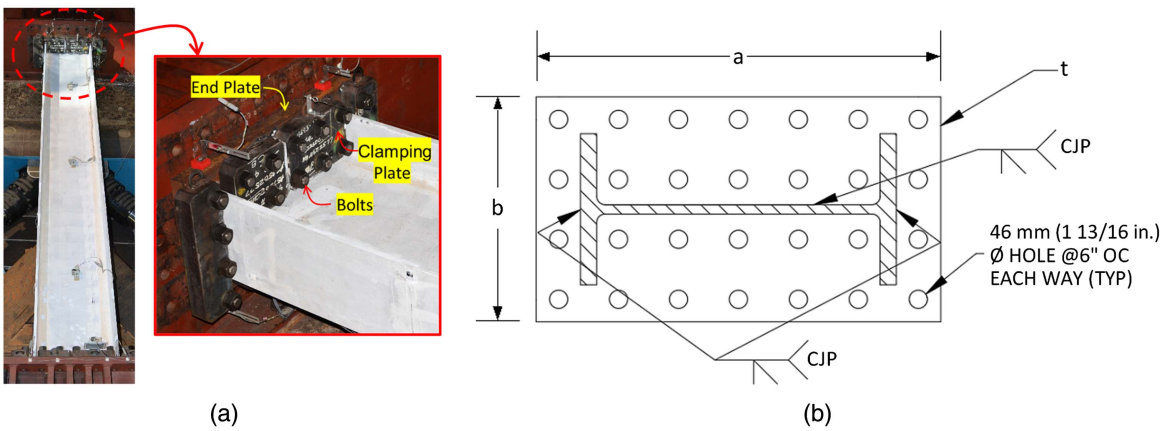

Fig. 2. Typical moment connection at specimen ends: (a) end connection details; and (b) end plate detail.

Table 3. Connection schedule

Specimen group	Shape	a (mm)	b (mm)	t (mm)	No. of bolts
1	W24 × 176	1,372	432	64	14
2	W24 × 131	1,372	432	64	14
3	W24 × 104	1,372	432	64	14
4	W24 × 84	1,372	432	64	14
5	W24 × 55	1,372	432	64	14
11	W24 × 176	1,029	572	76	24
12	W30 × 261	1,029	572	76	28
13	W30 × 173	1,029	572	76	28
14	W30 × 90	1,029	572	51	28
15	W18 × 192	724	572	51	20
16	W18 × 130	724	572	51	20
17	W18 × 76	724	572	51	20
22	W30 × 148	1,029	572	76	28
23	W18 × 60	724	572	51	20
24	W14 × 82	724	572	76	16
25	W14 × 53	724	572	76	16
26	W14 × 132	724	572	76	16
27	W24 × 84	1,029	572	51	24

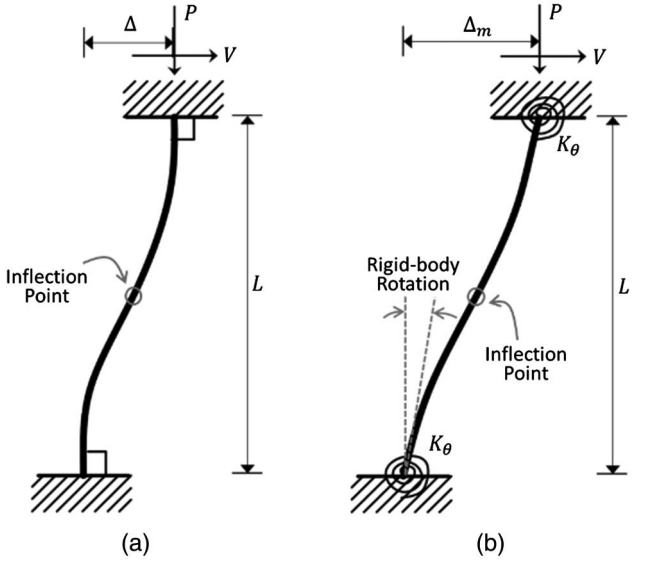

Fig. 3. Fixed-fixed beam-column with axial load and lateral drift: (a) ideal boundary conditions; and (b) actual boundary conditions.

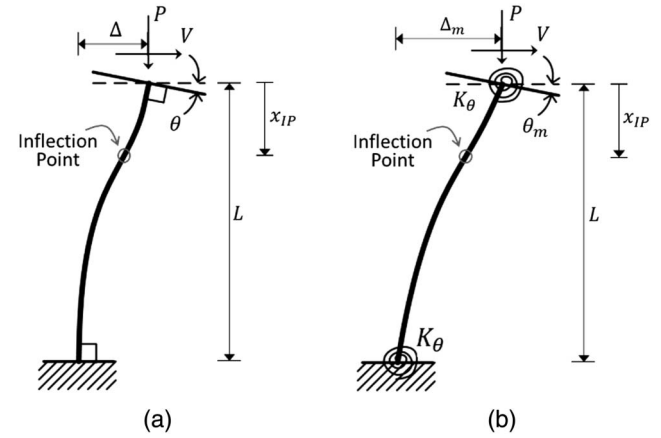

Fig. 4. Fixed-rotating beam-column with axial load, lateral drift, and top-end rotation: (a) ideal boundary conditions; and (b) actual boundary conditions.

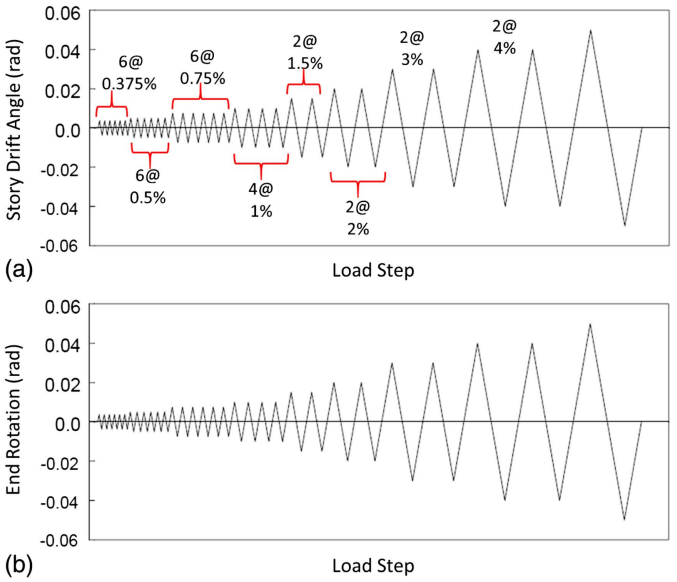

Fig. 5. Loading protocols: (a) AISC lateral story drift angle sequence; and (b) top end rotation sequence with $\xi_m = 1$.

Typical Beam-Column Responses

Hysteresis of the specimens is greatly influenced by beam-column yielding and buckling behaviors, which are characterized into three main modes defined by Ozkula et al. (2017): (1) symmetric flange local buckling mode, (2) antisymmetric local buckling mode, and (3) coupled buckling mode. The first mode is usually observed in stocky shallow (W14) columns, whereas the latter two modes are typical in deep column testing.

Figs. 6(a and b) show the antisymmetric local buckling mode and the associated lateral force-story drift response of Specimen 13M subjected to strong-axis bending with the fixed-fixed boundary conditions. FLB and WLB initiated simultaneously at 0.01 rad story drift angle, forming in-plane plastic hinges at both ends of the specimen. As a result, column axial shortening grew significantly, and the member flexural strength degraded drastically. The ductility capacity associated with this failure mode was sensitive to the axial force level.

Fig. 7(a) shows the deformed configuration of Specimen 11H-BC with the fixed-rotating boundary conditions; it involved both local buckling and lateral-torsional buckling, characterizing the coupled buckling mode. Inelastic deformation was limited at the moving end because the applied cyclic rotations reduced the moment there.

Subjected to weak-axis bending and having fixed-fixed boundary conditions, Specimen 6L with W24 × 131 shape exhibited excellent ductility; local buckling was not observed even at 0.07 rad story drift angle as shown in Fig. 8(a). Because neither local buckling nor lateral-torsional buckling occurred, column axial shortening and flexural strength degradation were not observed; the slight decrease in lateral strength at large drifts shown in Fig. 8(b) was due to the second-order effect from the applied axial compression.

Effects of Connection Flexibility and Challenges

The use of bolted end-plate connections to fix the specimens to reaction fixtures did not constitute ideal rigid boundary conditions.

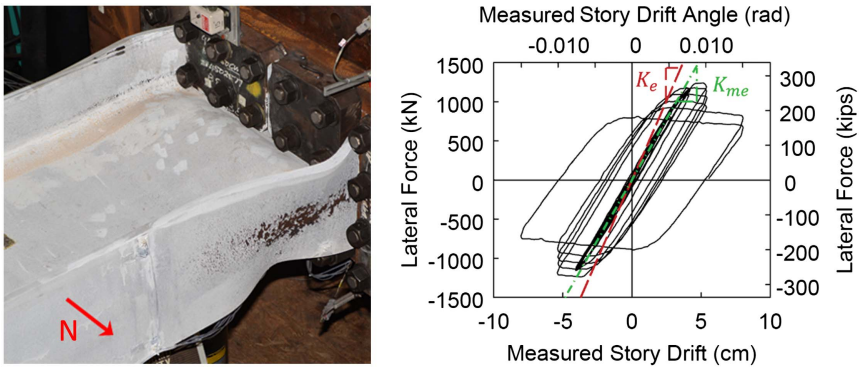

(a) (b)

Fig. 6. Specimen 13M (W30 × 173) with strong-axis bending: (a) antisymmetric local buckling mode at west end; and (b) global response.

(a)

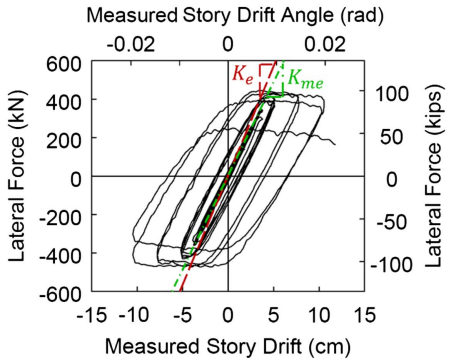

(b)

Fig. 7. Specimen 11H-BC (W24 × 176) with strong-axis bending: (a) coupled buckling mode; and (b) global response.

Due to out-of-plane flexibility of the end plates and elongation of the fastening rods, some relative rotations between the specimen ends and the reaction fixtures, i.e., connection rotations, were observed during the cyclic testing. Although Fig. 3(a) was the targeted fixed-fixed boundary conditions, end connection flexibility caused rigid-body rotation of the specimens as shown in Fig. 3(b). Because the measured column lateral drift, Δ_m, included a drift component contributed from the rigid-body movement due to the connection flexibility, the measured elastic lateral stiffness, K_{me}, obtained from linear regression of the elastic portion of the lateral force-story drift response could be significantly lower than a theoretical prediction, K_e, considering ideal rigid boundary conditions as shown in Fig. 3(a). Taking Specimen 13M for example, K_{me} is 23.1% smaller than K_e, as shown in Fig. 6(b).

For specimens with the fixed-rotating boundary conditions, not only the imposed lateral drifts but also the imposed end rotations included a component contributed from connection rotations [Fig. 4(b)]. Again, this caused the measured elastic responses to deviate from theoretical elastic responses of a beam-column with rigid end connections [Fig. 4(a)]. For Specimen 11H-BC, K_{me} is 13.4% smaller than K_e, as shown in Fig. 7(b).

For specimens subjected to weak-axis bending, connection rotations were negligible because the member weak-axis flexural stiffness was small in magnitudes relative to the rotational stiffness of the end connections. As a result, K_{me} and K_e of Specimen 6L are

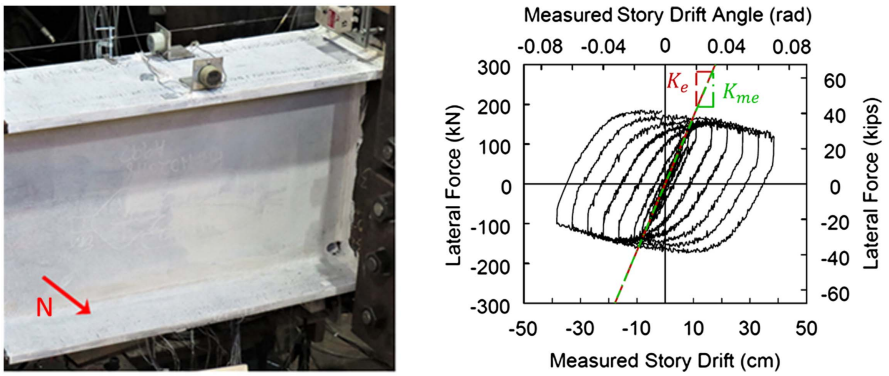

(a) (b)

Fig. 8. Specimen 6L (W24 × 131) with weak-axis bending: (a) yielding at west end; and (b) global response.

comparable, as shown in Fig. 8(b). Thus, this paper focuses on the effect of connection flexibility on beam-column tests with strong-axis bending. A procedure that removes the deformation component due to connection flexibility from the measured test responses is presented in the next section.

Proposed Data-Correction Procedure

Considering the flexibility of the end moment connections that causes rigid-body rotation of the specimens, the imposed (or measured) lateral drift at the moving end of the specimens, Δ_m, can be expressed

$$\Delta_m = \Delta_{me} + \Delta_{mc} + \Delta_{mp} \tag{2}$$

where Δ_{me} and Δ_{mp} = elastic and plastic components of the measured lateral drift due to column straining, respectively; and Δ_{mc} = component resulting from rigid-body rotation of the column due to connection flexibility at member ends. Removing Δ_{mc} from Δ_m gives the corrected story drift corresponding to ideal boundary conditions. Because it is difficult to measure Δ_{mc} experimentally due to the complex out-of-plane deformation of the end plates, this component was removed using the following procedure.

Assuming that Δ_{mc} remains elastic, $\Delta_{me} + \Delta_{mc}$ collectively represent the elastic component of Δ_m. Accordingly, the plastic component of Δ_m can be extracted as follows:

$$\Delta_{mp} = \Delta_m - \frac{V}{K_{me}} \tag{3}$$

where V = measured column shear (i.e., lateral force); and K_{me} = experimentally determined elastic stiffness (i.e., initial slope of the Δ_m versus V response). Corrected lateral drift due to the column deformation only is then the sum of the theoretical elastic drift, Δ_e, and the experimentally determined Δ_{mp}

$$\Delta = \Delta_e + \Delta_{mp} \tag{4}$$

where

$$\Delta_e = \frac{V}{K_e} \tag{5}$$

where K_e = best estimate of the elastic lateral stiffness and is represented by the theoretical lateral stiffness of a beam-column with ideal boundary conditions, i.e., rigid end connections. Substituting Eqs. (3) and (5) into Eq. (4) yields the final formula used to determine the corrected story drifts

$$\Delta = \Delta_e + \Delta_{mp} = \frac{V}{K_e} + \left(\Delta_m - \frac{V}{K_{me}}\right) \tag{6}$$

Eq. (6) can be used to correct the test responses of beam-column specimens; the resulting corrected story drifts can also be expressed in term of story angles as Δ/L. To provide a theoretical basis for the calculation of K_e for both the fixed-fixed and fixed-rotating boundary condition cases, a literature review of classical beam-column theories is discussed in the next section.

Beam-Column Theories: Members with Rigid End Connections

In an elastic analysis of a beam-column problem, Bernoulli-Euler theory assumes negligible shear deformation in calculating the member deflection. Considering a two-node member with end forces and corresponding degrees of freedom as shown in Fig. 9,

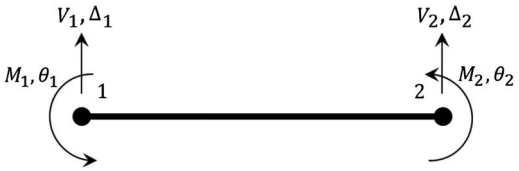

Fig. 9. Two-node member with four degrees of freedom.

the Euler lateral force-displacement relationship of a member with rigid end connections under a compressive axial force can be expressed as follows (Timoshenko and Gere 1961):

$$V_1 = \left[\frac{EIk^3 \sin kL}{2(1-\cos kL) - kL \sin kL}\right]\Delta_1 \tag{7}$$

where $k = \sqrt{P/EI}$, where P is axial load magnitude (i.e., absolute value of P); E = elastic modulus; and I = moment of inertia about the bending axis. Accordingly, the lateral stiffness is

$$\overline{K}_{11} = \frac{EIk^3 \sin kL}{2(1-\cos kL) - kL \sin kL} \tag{8}$$

where subscript 11 = position of the coefficient in the member flexural stiffness matrix.

To consider the effect of shear deformation on the beam-column lateral stiffness, Chugh (1977) transformed a flexibility matrix that accounts for shear deformation to derive the following lateral stiffness coefficient:

$$K'_{11} = \frac{EIk^3[\sin kL - \frac{2P}{kLGA_s}(1-\cos kL)]}{2(1+\frac{P}{GA_s})(1-\cos kL) - kL \sin kL} \tag{9}$$

where G = shear modulus; and A_s = effective shear area, accounting for the fact that shear stress and shear strain are not uniformly distributed over the member cross section. Defining

$$A_s = k_s A \tag{10}$$

where A = cross-sectional area, Cowper (1966) provided formulas for determining k_s, the Timoshenko shear coefficient, associated with various cross-sectional shapes. For a wide-flange member bent about its strong axis

$$k_s = \frac{10(1+\nu)(1+3m)^2}{A + \nu B + 30n^2(m+m^2) + 5\nu n^2(8m+9m^2)} \tag{11a}$$

where

$$A = 12 + 72m + 150m^2 + 90m^3$$
$$B = 11 + 66m + 135m^2 + 90m^3 \tag{11b}$$

where Poisson's ratio $\nu = 0.3$ for steel; $m = 2b_f t_f / h_0 t_w$; and $n = b_f / h_0$, where h_0 is the distance between the flange centroids. Alternatively, because shear stress distribution concentrates mostly in the web of the wide-flange member subjected to strong-axis bending, A_s is estimated as the web area of the shape in this study

$$A_s = (d - 2t_f)t_w \tag{12}$$

where d = cross-sectional depth. Fig. 10 shows the comparable results obtained from Eqs. (10) and (12). When the effect of axial force is not considered, Timoshenko beam theory can also reasonably approximate flexural stiffnesses (less than 6% difference from Timoshenko beam-column stiffnesses) of the wide-flange beam-column specimens tested in this program with strong-axis bending

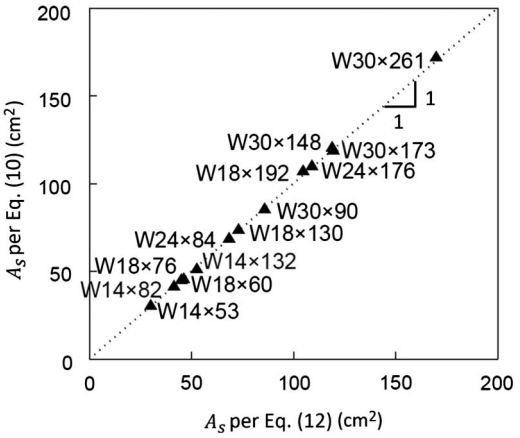

Fig. 10. Comparison of effective shear areas.

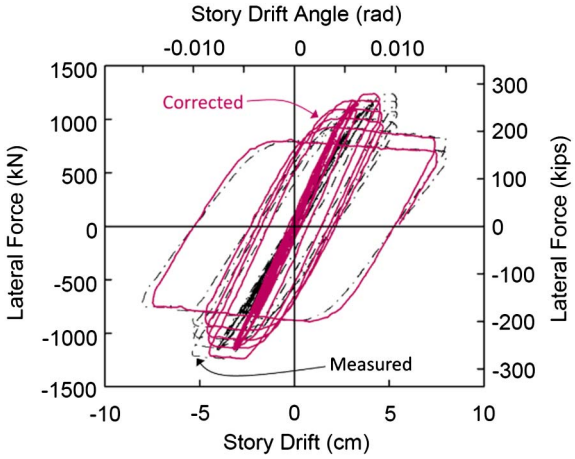

Fig. 11. Corrected versus measured hysteresis of Specimen 13M.

because the second-order effect can be small for this loading condition.

Considering properties and loading conditions of the deep wide-flange beam-column specimens tested in this program, the Euler beam-column theory [Eq. (8)] significantly overestimates the member lateral stiffnesses compared with the values obtained from the Timoshenko beam-column theory [Eq. (9)]. For instance, $\bar{K}_{11}$ and K'_{11} for the W30 × 173 member (Specimen 13M) are 53.24 and 40.35 kN/mm, respectively, showing 31.9% overestimation for the Euler equation. Therefore, to consider both the second-order effect and the shear deformation effect, the Timoshenko beam-column theory is used in this study to analyze elastic behavior of the deep beam-column specimens and calculate K_e.

Data Correction for Beam-Column Tests with Fixed-Fixed Boundary Conditions

Due to the symmetry of the fixed-fixed boundary conditions and the test setup, it was observed that the yielding and buckling patterns at both ends of the columns were very similar. Therefore, the inflection point can reasonably be assumed to remain at the midspan [Fig. 3(b)]. With this assumption [Fig. 3(a)], K_e for calculating the corrected story drift in Eq. (6) is as follows:

$$K_e = K'_{11} \tag{13}$$

An example correction of the lateral force-story drift response of Specimen 13M is shown in Fig. 11. The last column in Table 1 reports that the connection flexibility can reduce the lateral stiffness by 32.0% for the largest member (W30 × 261) tested. The stiffness reduction is lower for shallower and lighter members (e.g., W14 × 53 and W24 × 55).

Although the corrected story drift can be computed based on the aforementioned procedure, the equivalent rotational flexibility (or stiffness) of the member end connections is still unknown. Furthermore, the preceding procedure, which assumes that the inflection point is at the midspan, is not applicable for other boundary conditions. A procedure to overcome these issues is presented next.

Timoshenko Beam-Column Theory: Members with Rotationally Flexible End Connections

Data correction for specimens with fixed-rotating boundary conditions is not as simple compared with the fixed-fixed case because flexibility of end moment connections affects both the member stiffnesses and internal force distribution, i.e., inflection point location. Therefore, theoretical behavior of Timoshenko beam-columns with end rotational springs is presented next.

Many researchers have conducted studies of Timoshenko beam-columns using different methods (continuous, lumped, matrix analysis, finite-element method, and boundary element method, among others). Cheng and Pantelides (1988a, b) derived static and dynamic differential equations, stiffness matrix coefficients, and fixed-end forces of Timoshenko beam-columns that are supported on elastic media; the influence of a foundation parameter on the buckling modes was also investigated. Chung et al. (1993) studied dynamic behavior of Timoshenko beam-columns with rotationally flexible ends and intermediate concentrated masses, linear springs, and rotational springs; an exact solution method based on Hamilton's principle and the Laplace transform as well as the approximated Rayleigh-Ritz method were presented. Aristizabal-Ochoa (2004) studied a free vibration problem of a Timoshenko beam-column with generalized boundary conditions (i.e., with rotational and linear springs as well as lumped masses at both ends). In these studies, the main objectives of the dynamic analysis were to derive expressions for determining natural frequencies and corresponding mode shapes of the structural systems under consideration. Despite numerous studies on Timoshenko beam-columns with various boundary conditions, close-formed formulas for determining theoretical elastic flexural stiffnesses and internal force distribution in Timoshenko beam-columns with rotationally flexible ends are not available. To analytically quantify the effect of connection flexibility on both the imposed lateral drift and end rotation for specimens listed in Table 2, force-deformation relationships of a Timoshenko beam-column with rotationally flexible ends are derived as follows.

Assumptions

Fig. 12(a) shows an idealized configuration of the test specimens; connection flexibility at both ends of the member is represented as rotational springs with an equal stiffness K_θ:

$$K_\theta = \beta\left(\frac{EI}{L}\right) \tag{14}$$

where β = normalized rotational spring constant. Mechanical and mathematical assumptions typically made in elastic beam-column problems are applied in this derivation. Examples have been given by Cheng and Pantelides (1988a) and Aristizabal-Ochoa (2004). Fig. 12(b) shows the free-body diagram of a differential element

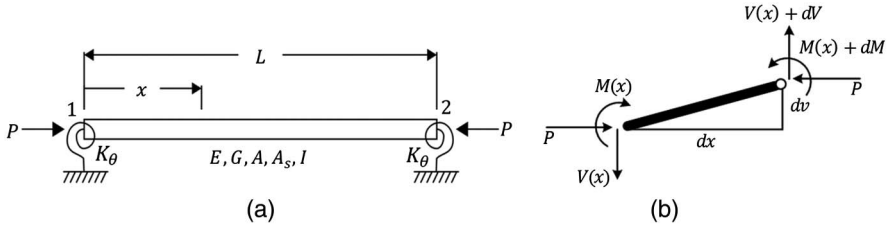

Fig. 12. Beam-column member with end rotational springs: (a) overall configuration; and (b) free-body of a differential segment.

located at x from End 1 of the member and the associated sign conventions that are assumed for the internal shear and moment.

Governing Differential Equations

Applying shear and moment equilibriums to the differential element gives

$$\frac{dV}{dx} = 0 \tag{15}$$

$$\frac{dM}{dx} + V(x) + P\frac{dv}{dx} = 0 \tag{16}$$

where v = lateral deflection; and α = flexural rotation. The Timoshenko force-deformation relationships for prismatic and homogeneous beam-columns can be expressed (Cheng and Pantelides 1988a)

$$V(x) + P\frac{dv}{dx} = GA_s\left[\frac{dv}{dx} - \alpha(x)\right] \tag{17}$$

$$M(x) = EI\frac{d\alpha}{dx} \tag{18}$$

From Eqs. (15)–(18), the following differential equation is derived:

$$EI\left(1 - \frac{P}{GA_s}\right)\frac{d^3\alpha}{dx^3} + P\frac{d\alpha}{dx} = 0 \tag{19}$$

The general solution for Eq. (19) can be found

$$\alpha(x) = C_1 \sin\frac{kx}{\sqrt{1-\mu}} + C_2 \cos\frac{kx}{\sqrt{1-\mu}} + C_3 \tag{20}$$

where $\mu = P/GA_s$. Substituting Eqs. (17), (18), and (20) into Eq. (16) and integrating once gives the lateral displacement equation

$$v(x) = \frac{1}{k\sqrt{1-\mu}}\left(-C_1 \cos\frac{kx}{\sqrt{1-\mu}} + C_2 \sin\frac{kx}{\sqrt{1-\mu}}\right) + C_3 x + C_4 \tag{21}$$

Boundary Conditions

To establish the member stiffness matrix, Eqs. (22)–(25) express four sets of boundary conditions corresponding to applications of a unit lateral displacement or a unit rotation at the external Nodes 1 and 2, respectively

$$v(0) = 1; \qquad v(L) = 0;$$
$$\frac{\beta EI}{L}[0 - \alpha(0)] = -EI\frac{d\alpha}{dx}\bigg|_{x=0}; \qquad \frac{\beta EI}{L}[0 - \alpha(L)] = EI\frac{d\alpha}{dx}\bigg|_{x=L} \tag{22}$$

$$v(0) = 0; \qquad v(L) = 0;$$
$$\frac{\beta EI}{L}[1 - \alpha(0)] = -EI\frac{d\alpha}{dx}\bigg|_{x=0}; \qquad \frac{\beta EI}{L}[0 - \alpha(L)] = EI\frac{d\alpha}{dx}\bigg|_{x=L} \tag{23}$$

$$v(0) = 0; \qquad v(L) = 1;$$
$$\frac{\beta EI}{L}[0 - \alpha(0)] = -EI\frac{d\alpha}{dx}\bigg|_{x=0}; \qquad \frac{\beta EI}{L}[0 - \alpha(L)] = EI\frac{d\alpha}{dx}\bigg|_{x=L} \tag{24}$$

$$v(0) = 0; \qquad v(L) = 0;$$
$$\frac{\beta EI}{L}[0 - \alpha(0)] = -EI\frac{d\alpha}{dx}\bigg|_{x=0}; \qquad \frac{\beta EI}{L}[1 - \alpha(L)] = EI\frac{d\alpha}{dx}\bigg|_{x=L} \tag{25}$$

For instance, Eq. (23) expresses the relationship between the spring moments and the member internal moments at ends when a unit rotation is applied at Node 1 as shown in Fig. 13.

Internal Shear and Moment Distributions

The expressions for $v(0)$, $v(L)$, $\alpha(0)$, and $\alpha(L)$ are determined using Eqs. (20) and (21). These expressions, when substituted into each boundary condition set, result in four homogeneous equations that can be solved to determine the coefficients C_1, C_2, C_3, and C_4 (Aristizabal-Ochoa 2004). Knowing these coefficients, Eqs. (20) and (21) can be substituted in Eqs. (17) and (18) to derive formulas of internal shear and moment distributions along the member. Denoting $v(0)$, $v(L)$, $\alpha(0)$, and $\alpha(L)$ as Δ_1, Δ_2, θ_1, and θ_2, respectively (Fig. 9 gives the symbol convention), internal force formulas corresponding to each boundary condition set are as follows:

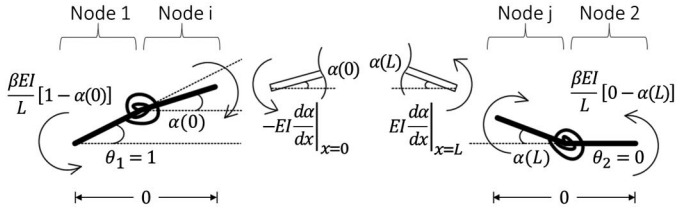

Fig. 13. Rotational spring moment and member internal moment relationship.

For $\Delta_1 = 1$, $\theta_1 = 0$, $\Delta_2 = 0$, and $\theta_2 = 0$, they are

$$V_{\Delta_1}(x) = -\frac{EIk^3}{\Psi}\{2kL(\sqrt{1-\mu})\beta c - [(kL)^2 - (1-\mu)\beta^2]s\}$$
$$M_{\Delta_1}(x) = -\frac{2EIk^2\beta}{\Psi}\left[kL\cos\frac{kL}{2\sqrt{1-\mu}} + (\sqrt{1-\mu})\beta\sin\frac{kL}{2\sqrt{1-\mu}}\right]\sin\frac{k(L-2x)}{2\sqrt{1-\mu}} \quad (26)$$

For $\Delta_1 = 0$, $\theta_1 = 1$, $\Delta_2 = 0$, and $\theta_2 = 0$, they are

$$V_{\theta_1}(x) = -\frac{EIk^2\beta}{\Psi}[kLs + (\sqrt{1-\mu})\beta(1-c)]$$
$$M_{\theta_1}(x) = \frac{EIk\beta}{\Psi}\left\{kL(\sqrt{1-\mu})\beta\cos\frac{k(L-x)}{\sqrt{1-\mu}} - [(kL)^2+\beta]\sin\frac{k(L-x)}{\sqrt{1-\mu}} - \beta\sin\frac{kx}{\sqrt{1-\mu}}\right\} \quad (27)$$

For $\Delta_1 = 0$, $\theta_1 = 0$, $\Delta_2 = 1$, and $\theta_2 = 0$, it is

$$V_{\Delta_2}(x) = -V_{\Delta_1}(x)$$
$$M_{\Delta_2}(x) = -M_{\Delta_1}(x) \quad (28)$$

For $\Delta_1 = 0$, $\theta_1 = 0$, $\Delta_2 = 0$, and $\theta_2 = 1$, they are

$$V_{\theta_2}(x) = V_{\theta_1}(x)$$
$$M_{\theta_2}(x) = -\frac{EIk\beta}{\Psi}\left\{kL(\sqrt{1-\mu})\beta\cos\frac{kx}{\sqrt{1-\mu}} - \left[(kL)^2+\beta\right]\sin\frac{kx}{\sqrt{1-\mu}} - \beta\sin\frac{k(L-x)}{\sqrt{1-\mu}}\right\} \quad (29)$$

where $c = \cos(kL/\sqrt{1-\mu})$; $s = \sin(kL/\sqrt{1-\mu})$; and

$$\Psi = 2(\sqrt{1-\mu})\beta^2\left\{1 - \left[1 + \frac{(kL)^2}{\beta}\right]c\right\} - kL[(1-\mu)\beta^2 - 2\beta - (kL)^2]s \quad (30)$$

Stiffness Matrix

Setting x to either 0 or L, $V_{\Delta_1}(0)$, $M_{\Delta_1}(0)$, $V_{\Delta_1}(L)$, and $M_{\Delta_1}(L)$, can be determined using Eq. (26) to establish stiffness coefficients in the first column of the Timoshenko beam-column stiffness matrix, $[K]$.

$$\begin{Bmatrix} V_1 \\ M_1 \\ V_2 \\ M_2 \end{Bmatrix} = \begin{bmatrix} K_{11} & K_{12} & K_{13} & K_{14} \\ K_{21} & K_{22} & K_{23} & K_{24} \\ K_{31} & K_{32} & K_{33} & K_{34} \\ K_{41} & K_{42} & K_{43} & K_{44} \end{bmatrix} \begin{Bmatrix} \Delta_1 \\ \theta_1 \\ \Delta_2 \\ \theta_2 \end{Bmatrix} \quad (31)$$

Similarly, the same process can be carried out using Eqs. (27)–(29) to establish the remaining coefficients in the stiffness matrix. The stiffness coefficients are

$$K_{11} = \frac{EIk^3}{\Psi}\{2kL(\sqrt{1-\mu})\beta c - [(kL)^2 - (1-\mu)\beta^2]s\}$$
$$K_{12} = \frac{EIk^2\beta}{\Psi}[kLs + (\sqrt{1-\mu})\beta(1-c)]$$
$$K_{22} = \frac{EIk\beta}{\Psi}\{[(kL)^2+\beta]s - kL(\sqrt{1-\mu})\beta c\}$$
$$K_{24} = \frac{EIk\beta^2}{\Psi}[kL(\sqrt{1-\mu}) - s]$$
$$-K_{13} = -K_{31} = K_{33} = K_{11}$$
$$-K_{32} = -K_{23} = -K_{43} = -K_{34} = K_{41} = K_{14} = K_{21} = K_{12}$$
$$K_{44} = K_{22}$$
$$K_{42} = K_{24} \quad (32)$$

With these stiffness coefficient expressions, flexibility of the end moment connections can be quantified in term of an equivalent end rotational spring stiffness. For fixed-fixed specimens, for instance, the relationship between the column shear and the measured lateral drift in the elastic range can be expressed as follows:

$$V = K_{11}\Delta_m \quad (33)$$

Eq. (33) can be calibrated with the elastic portion of the measured lateral force-story drift test responses to determine β and associated K_θ [Eq. (14)]; the calculated values of β for the fixed-fixed boundary condition test specimens are listed in Table 1. It is difficult to achieve a rigid connection, i.e., $\beta \to \infty$, in real steel construction. Commentary of AISC 360 (AISC 2016c) states that it is acceptable to consider a connection to be fully restrained, i.e., able to maintain the angle between two members, when $\beta \geq 20$. A connection is considered simple and can be modeled as a hinge, i.e., it rotates without developing moment, when $\beta \leq 2$. Considering β values listed in Table 1, the test end moment connections behaved in a more flexible manner when a low level of axial compression was applied to the specimen: β values associated with low-axial load specimens were lower than those associated with medium- and high-axial-load specimens. In the next section, further application of the derived Timoshenko beam-column formulas to correct test data for fixed-rotating specimens is discussed.

Data Correction for Beam-Column Tests with Fixed-Rotating Boundary Conditions

Because the end moments at the fixed and rotating ends were not the same in magnitude, connection rotation at each column end also

differed in magnitude. Consequently, in addition to the applied end rotation at the moving end, connection flexibility also influenced the location of inflection point in the specimens. The following steps determine K_e for fixed-rotating specimens, which is needed in Eq. (6) to remove the effect of connection flexibility from the lateral drift responses: (1) determine the equivalent end rotational spring stiffness and locate the inflection point in the specimens; (2) based on the determined inflection point location, calculate an equivalent moving-end rotation assuming both column-end connections are rigid; and (3) calculate K_e based on the equivalent moving-end rotation determined in Step 2.

Step 1: Determine the End Rotational Spring Stiffness and Inflection Point Location

By idealizing the connection flexibility at both ends of the specimens as rotational springs with an identical equivalent stiffness, $\beta(EI/L)$, Eq. (34) expresses the theoretical elastic lateral stiffness relationship of a fixed-rotating beam-column with rotationally flexible ends

$$V = (K_{11} - \frac{\xi_m}{L} K_{12})\Delta_m \tag{34}$$

This equation is derived by setting $\Delta_1 = \Delta_m$, $\theta_1 = -\theta_m = -\xi_m(\Delta_m/L)$, and $\Delta_2 = \theta_2 = 0$ in the first equation in Eq. (31). Eq. (34) is then calibrated with the measured lateral force-story drift elastic response to back-calculate β. Once β is determined, internal moment along the member can be expressed using the superposition principle

$$M(x) = M_{\Delta_1}(x)\Delta_m - M_{\theta_1}(x)\theta_m = [M_{\Delta_1}(x) - \frac{\xi_m}{L} M_{\theta_1}(x)]\Delta_m \tag{35}$$

where x is measured from the moving end. Setting Eq. (35) to zero and solving for x give the inflection point location, x_{IP}, in the specimen. Table 2 gives the calculated x_{IP} values for the three test specimens.

Step 2: Determine an Equivalent Moving-End Rotation

To eliminate the effect of rigid-body rotation caused by connection flexibility that contributed to both the measured lateral drift (Δ_m) and end rotation (θ_m) as shown in Fig. 4(b), the specimen is assumed to have ideal fixed-rotating boundary conditions, i.e., rigid end connections as shown in Fig. 4(a), and sustain an equivalent moving-end rotation of

$$\theta = \xi\left(\frac{\Delta}{L}\right) \tag{36}$$

Essentially, if the specimen sustained θ and Δ at the moving end with ideal boundary conditions, it would have the same inflection point location as if it sustained θ_m and Δ_m with flexible end connections; both the ideal and real configurations are equivalent. The equivalent moving-end rotation, θ, is determined as follows.

Similar to Eq. (35), Eq. (37) expresses the theoretical internal moment along a beam-column with ideal fixed-rotating boundary conditions

$$M'(x) = [M'_{\Delta_1}(x) - \frac{\xi}{L} M'_{\theta_1}(x)]\Delta \tag{37}$$

where

$$M'_{\Delta_1}(x) = \frac{-2EIk^2(\sqrt{1-\mu})\sin\frac{kL}{2\sqrt{1-\mu}}\sin\frac{k(L-2x)}{2\sqrt{1-\mu}}}{2\sqrt{1-\mu}(1-c) - kL(1-\mu)s} \tag{38}$$

$$M'_{\theta_1}(x) = \frac{EIk\{kL(\sqrt{1-\mu})\cos\frac{k(L-x)}{\sqrt{1-\mu}} - \sin\frac{k(L-x)}{\sqrt{1-\mu}} - \sin\frac{kx}{\sqrt{1-\mu}}\}}{2\sqrt{1-\mu}(1-c) - kL(1-\mu)s} \tag{39}$$

Eqs. (38) and (39) are obtained by setting $\beta \to \infty$ in Eqs. (26) and (27) for $M_{\Delta_1}(x)$ and $M_{\theta_1}(x)$.

Substituting x_{IP} determined in Step 1 into Eq. (37) gives

$$M'(x_{\mathrm{IP}}) = [M'_{\Delta_1}(x_{\mathrm{IP}}) - \frac{\xi}{L} M'_{\theta_1}(x_{\mathrm{IP}})]\Delta \tag{40}$$

Accordingly, ξ can be calculated such that $M'(x_{\mathrm{IP}}) = 0$ to make the inflection point location of the ideal configuration identical to that of the actual configuration. The value of θ is then calculated per Eq. (36). Table 2 gives the calculated ξ values.

Step 3: Calculate K_e

Eq. (41) expresses the theoretical lateral force-story drift relationship of the specimens with equivalent ideal fixed-rotating boundary conditions

$$V = (K'_{11} - \frac{\xi}{L} K'_{12})\Delta \tag{41}$$

Thus, K_e based on the Timoshenko theory considering both shearing and second-order effects becomes

$$K_e = K'_{11} - \frac{\xi}{L} K'_{12} \tag{42}$$

where K'_{11} is calculated as in Eq. (9) and (Chugh 1977)

$$K'_{12} = \frac{EIk^2(1-\cos kL)}{2(1+\frac{P}{GA_s})(1-\cos kL) - kL\sin kL} \tag{43}$$

The calculated K_e is then used in Eq. (6) to compute the corrected drift.

An example correction of the lateral force-story drift response of Specimen 11H-BC is shown in Fig. 14. Calculated values of K_{me} and K_e are 9.75 and 11.27 kN/mm, respectively, showing that the connection flexibility reduces the lateral stiffness by 13.4%. Table 2

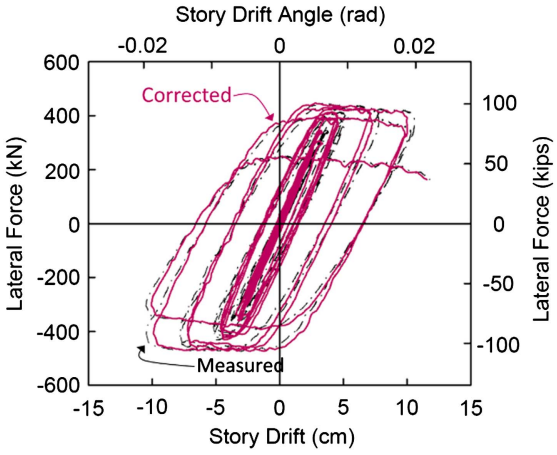

Fig. 14. Corrected versus measured hysteresis of Specimen 11H-BC.

J. Struct. Eng., 2020, 146(3): 04019230

summarizes key variables associated with this drift-correction procedure for each fixed-rotating specimen.

Summary and Conclusions

In steel wide-flange beam-column cyclic testing, the measured responses are sensitive to flexibility of the fully restrained moment connections that fix the specimen ends. Although it is feasible to design end moment connections to reach near full fixity in testing of small-size specimens, the task becomes difficult when testing large-size members at full-scale level. Correspondingly, the unavoidable connection rotations become another variable that influences the test responses, hindering investigation of parameters of interest in the test program. Utilizing theoretical elastic Timoshenko beam-column force-deformation relationships, a data-reduction procedure has been proposed to remove the effect of connection flexibility from the measured beam-column responses. Stiffness formulas available in literature can be used to correct the test data for beam-column specimens tested with the fixed-fixed boundary conditions. Built upon existing theories, further derivations of Timoshenko beam-column force-deformation relationships have been presented in this paper to correct test data for beam-column specimens tested with fixed-rotating boundary conditions.

Acknowledgments

Funding for this research was provided by the NEHRP Consultants Joint Venture Earthquake, Structural, and Engineering Research for the National Institute of Standards and Technology (NIST). American Institute of Steel Construction and Herrick Corporation donated the test specimens. Mr. J. O. Malley from Degenkolb Engineers chaired the Project Technical Committee, and Ms. A. Hortacsu from Applied Technology Council served as the project manager. The authors would like to acknowledge Dr. J. L. Harris III from NIST for reviewing this paper.

References

AISC. 2016a. *Prequalified connections for special and intermediate steel moment frames for seismic applications*. ANSI/AISC 358. Chicago: AISC.

AISC. 2016b. *Seismic provisions for structural steel building*. ANSI/AISC 341. Chicago: AISC.

AISC. 2016c. *Specification for structural steel buildings*. ANSI/AISC 360. Chicago: AISC.

Aristizabal-Ochoa, J. D. 2004. "Timoshenko beam-column with generalized end conditions and nonclassical modes of vibration of shear beams." *J. Eng. Mech.* 130 (10): 1151–1159. https://doi.org/10.1061/(ASCE)0733-9399(2004)130:10(1151).

ASCE. 2016. *Minimum design loads and associated criteria for buildings and other structures*. ASCE/SEI 7. Reston, VA: ASCE.

ASTM. 2017. *Standard specification for quenched and tempered alloy steel bolts, studs, and other externally threaded fasteners*. ASTM A354. West Conshohocken, PA: ASTM.

ASTM. 2018. *Standard specification for high-strength low-alloy columbium-vanadium structural steel*. ASTM A572. West Conshohocken, PA: ASTM.

Chansuk, P., G. Ozkula, and C.-M. Uang. 2018. *Seismic behavior and design of deep, slender wide-flange structural steel beam-columns: Phase 2 testing*. Rep. No. SSRP-18/02. San Diego: Univ. of California.

Cheng, F. Y., and C. P. Pantelides. 1988a. "Dynamic Timoshenko beam-columns on elastic media." *J. Struct. Eng.* 114 (7): 1524–1550. https://doi.org/10.1061/(ASCE)0733-9445(1988)114:7(1524).

Cheng, F. Y., and C. P. Pantelides. 1988b. "Static Timoshenko beam-columns on elastic media." *J. Struct. Eng.* 114 (5): 1152–1172. https://doi.org/10.1061/(ASCE)0733-9445(1988)114:5(1152).

Chugh, A. K. 1977. "Stiffness matrix for a beam element including transverse shear and axial force effects." *Int. J. Numer. Methods Eng.* 11 (11): 1681–1697. https://doi.org/10.1002/nme.1620111105.

Chung, J. H., W. H. Joo, and K. C. Kim. 1993. "Vibration and dynamic sensitivity analysis of a Timoshenko beam-column with elastically restrained ends and intermediate constraints." *J. Sound Vib.* 167 (2): 209–221. https://doi.org/10.1006/jsvi.1993.1331.

Cowper, G. R. 1966. "The shear coefficient in Timoshenko's beam theory." *J. Appl. Mech.* 33 (2): 335–340. https://doi.org/10.1115/1.3625046.

Harris, J. L., and M. S. Speicher. 2015. *Assessment of first generation performance-based seismic design methods for new steel buildings: volume 1: Special moment frames*. NIST TN 1863-1. Gaithersburg, MD: NIST.

Newell, J. D., and C.-M. Uang. 2008. "Cyclic behavior of steel wide-flange columns subjected to large drift." *J. Struct. Eng.* 134 (8): 1334–1342. https://doi.org/10.1061/(ASCE)0733-9445(2008)134:8(1334).

NIST. 2011. *Research plan for the study of seismic behavior and design of deep, slender, wide-flange structural steel-beam-column members*. NIST-GCR-11-917-13. Gaithersburg, MD: NIST.

Ozkula, G., J. Harris, and C.-M. Uang. 2017. "Classifying cyclic buckling modes of steel wide-flange columns under cyclic loading." In *Proc., Structures Congress*. Reston, VA: ASCE.

Ozkula, G., and C.-M. Uang. 2015. *Seismic behavior and design of deep, slender wide-flange structural steel beam-columns: Phase 1 testing*. Rep. No. SSRP-15/06. San Diego: Univ. of California.

Ozkula, G., and C.-M. Uang. 2017. "Observations from cyclic tests on deep, wide-flange beam-columns." *Eng. J.* 54 (1): 45–59.

Timoshenko, S. P., and J. M. Gere. 1961. *Theory of elastic stability*. 2nd ed. New York: McGraw-Hill.